Asymptotic theory for diffusive electromagnetic imaging

Jean Virieux,[1] Carlos Flores-Luna[1,2] and Dominique Gibert[3]

[1] *Institut de Géodynamique, UNSA Rue Albert Einstein, 06560 Valbonne, France*
[2] *CICESE, Depto. Geofisica Aplicada KM 107 Carretera. Tijuana-Ensenada, Ensenada 22800, Baja California, Mexico*
[3] *Geosciences Rennes, Rennes I Avenue Général Leclerc, 35042 Rennes cédex, France*

SUMMARY

We propose an asymptotic theory for diffusive electromagnetic imaging. Three steps are required to perform this imaging. (1) A high-frequency solution is first constructed which mimics the one usually found in wave-propagation phenomena. (2) This solution, valid for a smooth continuous description of the resistivity in the medium, is used in a first-order Born approximation leading to a linear relation between the resistivity perturbation of the subsurface and the perturbation of the electric signal obtained at the free surface. (3) This linear relation is asymptotically inverted by using an iterative quasi-Newtonian inversion based on a least-squares criterion developed by Jin *et al.* (1992). Although the extension to smooth heterogeneous reference medium is possible, we have only tested the inversion scheme for homogeneous reference media as Zhdanov & Frenkel (1983) previously did with another method.

Key words: electrical conductivity, electromagnetic surveys, inversion.

INTRODUCTION

Recovering conductivity information in the Earth is a difficult task because the electromagnetic response is mainly controlled by a diffusion process broadening the signal. Many attempts have encountered limited success (Weidelt 1972, 1975; Barnett 1984; Tripp, Hohmann & Swift 1984; Smith 1988; Tarits 1989) associated with the difficult task of locating the conductivity anomaly responsible for the electromagnetic signal observed at the free surface. In many papers (Zhdanov & Frenkel 1983; Zhdanov 1988; Zhdanov & Booker 1993; Zhdanov & Keller 1994), Zhdanov and his coworkers have proposed a 'reverse' continuation of the field in a manner similar to seismic-wave migration. Lee, McMechan & Aiken (1987) and Levy, Oldenburg & Wang (1988) have applied seismic techniques for layered media with complex matrices for propagator leading to the difficulty of strong variations of the amplitudes. In both cases, the complete Green function is used and one may think that the success of many seismic migration techniques based on the separation of traveltime fitting and amplitude adjustment has not yet been exploited.

Does a way exist to construct an asymptotic solution for the diffusion electromagnetic problem which will be helpful in an 'electromagnetic' imaging? It will be a more direct way than to convert electromagnetic data into pseudo-seismic data in order to use standard techniques of seismic imaging. Recent papers by Lee, Liu & Morrison (1989), Gilbert & Virieux (1991) and Lee & Xie (1993) have suggested this latter strategy to increase the stability and accuracy of electromagnetic imaging. In a recent paper, Nekut (1994) has achieved this direct strategy for phase/traveltime interpretation.

We shall show that, indeed, it is possible to construct a solution which might be useful for least-squares inversion of electromagnetic data. The inversion we propose comes directly from recent works on efficient techniques to construct seismic images (see Jin *et al.* 1992, for cited references).

SOLUTION FOR A HOMOGENEOUS MEDIUM

This section specifies our equations and the construction of a solution for a homogeneous medium. This construction will be such that extension to inhomogeneous media is possible.

In a 3-D medium with conductivity σ_0 and permeability μ_0 without sources of displacement current, Maxwell equations for the electric field **E** and the magnetic susceptibility field **H** reduce to the following equations

$$\frac{\partial \mathbf{H}}{\partial t} = -\frac{1}{\mu_0} \nabla \times \mathbf{E},$$

$$\sigma_0 \mathbf{E} + \epsilon \frac{\partial \mathbf{E}}{\partial t} = \nabla \times \mathbf{H}, \tag{1}$$

where $\times$ denotes the cross product. For the transverse electric mode (TE), the electric field **E** has one constant direction which can be defined as the y-direction. The vector

E can be written $(0, E_y, 0)$ and we assume invariance in the y-direction. The magnetic susceptibility field **H** has only two components $(H_x, 0, H_z)$. We found

$$\frac{\partial H_x}{\partial t} = \frac{1}{\mu_0} \frac{\partial E_y}{\partial z},$$

$$\frac{\partial H_z}{\partial t} = -\frac{1}{\mu_0} \frac{\partial E_y}{\partial x}, \tag{2}$$

$$\sigma_0 E_y + \epsilon \frac{\partial E_y}{\partial t} = \frac{\partial H_x}{\partial z} - \frac{\partial H_z}{\partial x}.$$

For the transverse magnetic mode (TM), similar equations are obtained. This system of equations shows similarity but also differences with the system of equations for *SH* motion in an elastic medium. The intrinsic difference comes from the term $\sigma_0 E_y$ which introduces the diffusion. The system (2) can be transformed into the telegraph equation

$$\sigma_0 \frac{\partial E_y}{\partial t} + \epsilon \frac{\partial^2 E_y}{\partial t^2} = \frac{1}{\mu_0} \left(\frac{\partial^2 E_y}{\partial x^2} + \frac{\partial^2 E_y}{\partial z^2} \right), \tag{3}$$

which might be considered as an extension of the wave equation with the extra diffusive term $\sigma_0 \partial E_y / \partial t$. Although transformation exists to convert diffusion into propagation (Levy *et al.* 1988; Lee *et al.* 1989; Gibert & Virieux 1991), deep differences arising from the diffusive extra term are found which prevent a straightforward parallelism between techniques used in propagation and in diffusion.

The separation between the TE mode and the TM mode is not more valid at interfaces of zeroth-order discontinuity for the conductivity (Wait 1981). Boundary conditions have to be applied which couple the TM and TE modes. We do not consider interfaces in the following and we shall consider only a smooth continuous medium necessary for our asymptotic imaging.

Going to the Fourier domain with the following sign convention given by

$$f(t) = \frac{1}{2\pi} \int_{-\infty}^{+\infty} f(\omega) e^{-i\omega t} \, d\omega \tag{4}$$

and keeping the same notation for the Fourier transform of the function E_y, we deduce the Helmholtz equation:

$$-(i\sigma_0 \omega + \omega^2 \epsilon) E_y = \frac{1}{\mu_0} \left(\frac{\partial^2 E_y}{\partial x^2} + \frac{\partial^2 E_y}{\partial z^2} \right) \tag{5}$$

again similar but different to the one deduced from wave equation. At high frequency, the diffusive term in $\sigma_0 \omega$ can be neglected compared with $\epsilon \omega^2$ and we are going back strictly speaking to the wave equation used for instance in high-frequency georadar imaging (Davis, Lytle & Laine 1979; Radcliff & Balanis 1981). Here we are interested in a lower frequency range where the term in $\epsilon \omega^2$ can be neglected instead, and eq. (5) reduces to

$$i\omega \sigma_0 \mu_0 E_y + \Delta E_y = 0. \tag{6}$$

A generating solution of this equation is a complex plane

wave $\exp(\mathbf{k} \cdot \mathbf{x})$ with $-i\omega \sigma_0 \mu_0 = k^2$. The selection of the square root of $-i$ is such that the plane-wave amplitude should decrease with distance.

Let us briefly recall what are solutions in a homogeneous medium for an impulsive signal $-4\pi\delta(t)$. Let us consider a line source. The solution will be

$$\frac{1}{t} e^{-\mu_0 \sigma_0 r^2 / 4t} H(t), \tag{7}$$

whose Fourier transform is $2K_0(\sqrt{-i\omega}\sqrt{\mu_0 \sigma_0} \, r)$. The function K_0 is the modified Bessel function of zero order. Taking the approximation of the function K_0 for large arguments, an asymptotic solution can be written for the 2-D case as follows

$$\sqrt{2\pi} \frac{1}{\sqrt{\sqrt{-i\omega}\sqrt{\mu_0 \sigma_0}}} \frac{1}{\sqrt{r}} e^{-\sqrt{-i\omega}\sqrt{\mu_0 \sigma_0} \, r}, \tag{8}$$

where r is the distance between the line source $(0, 0)$ and the receiver (x, z) and $H(t)$ is the Heaviside function. The time at which the solution is maximum is $t = \mu_0 \sigma_0 r^2 / 4$ while the mean square distance of the diffusion from the source at time t is $4t / \mu_0 \sigma_0$ (Carslaw & Jaeger 1978, p. 256). In practical applications, the penetration depth of diffusive electromagnetic signal from the surface of the Earth ranges from a few kilometres up to many hundreds of kilometres for commonly used frequencies (Cagniard 1953).

The solution (8) must be analysed carefully when compared with the exact solution (7). We must underline that we have only constructed an approximate asymptotic solution in the 2-D homogeneous case. Moreover a frequency-dependent scaling factor $1/\sqrt{\sqrt{-i\omega}}$ appears in the solution. This factor came for the spatial extension of the source. One can find that a similar factor $1/\sqrt{i\omega}$ appears in the 2-D asymptotic solution of the wave propagation corresponding to the Hilbert transform. As for the wave propagation, this factor will be retained during our construction of an asymptotic solution for a smoothly varying medium. Then, it will be introduced at the end of the procedure in the final solution to take into account the geometry of the problem as done for wave propagation (Bleistein 1984).

Obviously, this solution has a specific damping and oscillating factor we hope to observe for a smooth inhomogeneous medium. Following the basic idea leading to the high-frequency approximation for the wave-equation solution (Aki & Richards 1980), we are going to construct an asymptotic solution for the diffusion equation.

We must underline that similar exact solutions can be constructed for 1-D and 3-D geometries. These solutions in the Fourier domain display the same specific damping and oscillating factor without any approximation which was not the case for 2-D geometry. Consequently, the asymptotic solution we are going to construct is the exact solution for the homogeneous 1-D and 3-D cases, while it is only an approximation for the homogeneous 2-D cases. This means that the 2-D geometry is the worst situation to be considered for asymptotic diffraction tomographic reconstruction. The reconstruction method we propose will use exact Green functions when the 1-D or 3-D background media are homogeneous. This validates the use of the asymptotic

solution and our numerical attempt to estimate the accuracy of 2-D geometrical reconstructions.

ASYMPTOTIC SOLUTION FOR A SMOOTH MEDIUM

Let us assume now that the medium has a smooth variation of the conductivity $\sigma(\mathbf{x})$. We look for a solution in the frequency domain which behaves as

$$e^{-\sqrt{-i\omega}\,\tau(\mathbf{x})} \sum_{k=0}^{+\infty} \frac{A_k(\mathbf{x})}{(\sqrt{-i\omega})^k}. \tag{9}$$

This ansatz for the solution is the one used in the ray theory except that the $i\omega$ term for wave propagation has been replaced by $-\sqrt{-i\omega}$ for diffusive transport. It has been previously proposed by Tikhonov (1965) on a purely theoretical basis. This term has no obvious property in the Fourier domain as the translation property of the exponential terms. Nevertheless, we have already constructed an analytical solution in the previous section with this factor. The function τ will be called the pseudo-phase function following previous works on the link between diffusion and propagation equations (Lee *et al.* 1989; Gibert & Virieux 1991). The dimension of the pseudo-phase is the square root of time.

For the wave-propagation equation, many other ansatz have been suggested to take into account specific geometries: ray theory singularities at caustics (Ludwig 1966), evanescent waves (Choudhary & Felsen 1973). A seismological classification has been given by Chapman (1985), while a review of different ansatz has been given by Borovikov & Kinber (1974). These different ansatz show the interest in developing specific asymptotic solutions for each problem at hand.

Inserting the ansatz (9) in eq. (6) which is still valid for a continuous inhomogeneous conductivity $\sigma(x)$, we deduce series of equations in powers of $\sqrt{-i\omega}$:

$$(\sqrt{-i\omega})^2 \quad (\nabla\tau)^2 = \sigma(\mathbf{x})\mu_0$$

$$\sqrt{-i\omega} \quad A_0\nabla^2\tau + 2\nabla A_0 \cdot \nabla\tau = 0 \tag{10}$$

$$\sqrt{-i\omega}^{(1-k)} \quad \nabla^2 A_{k-1} - A_k\nabla^2\tau + 2\nabla A_k \cdot \nabla\tau = 0 \quad k >= 1.$$

The first two equations retain our attention because solving them will give the pseudo-phase $\tau(\mathbf{x})$ and the amplitude $A_0(\mathbf{x})$ used for the zero-order term of the solution. These are identical to both the eikonal and the transport equations used for ray tracing of seismic waves and permit us to compute $\tau(\mathbf{x})$ and $A_0(\mathbf{x})$ with any standard ray-tracing program (see Lambaré 1992, for an example of efficient ray tracing used for imaging). The intrinsic property of the diffusion is contained in the ansatz we have taken. The signal has its amplitude split in two parts: geometrical spreading A_0 and a 'bulk' attenuation contained in the pseudo-phase function. These two effects contribute in a different manner to the electromagnetic diffusion amplitude.

Let us compare more precisely the zero-order term of eq. (9) with its propagative equivalent for which the traveltime of the wave is taken as T. For a Dirac source at

the origin, the diffusive and propagation solutions are, respectively,

$$e^{-\sqrt{-i\omega}\,\tau(\mathbf{x})}A_0(\mathbf{x}) \to A_0(\mathbf{x})\frac{\tau(\mathbf{x})}{2\sqrt{\pi t^3}}e^{-\tau^2(\mathbf{x})/4t}H(t),$$

$$e^{i\omega T(\mathbf{x})}A_0(\mathbf{x}) \to A_0(\mathbf{x})\delta[t - T(\mathbf{x})], \tag{11}$$

in a 3-D medium. These solutions have a very simple geometrical interpretation. The wave solution is the delta source signal shifted by the traveltime T and scaled by A_0 (Fig. 1). The diffusive solution is more complex to analyse: the delta source signal is transformed into a localized damped function maximum at $\tau^2/6$ (Fig. 2) which is similar to a phase shift although the diffusive energy stays around the source. The geometrical effect of the 2-D medium will add a tail to both signals, while reducing down to the 1-D geometry again deforms the signal. The geometry of medium influences the propagation and diffusion of the signal as summarized in Fig. 1 and Fig. 2. The diffusion solution (11) adds an extra difficulty because it exhibits a time decrease of $1/\sqrt{t^3}$ which is converted in a $1/t$ decrease in the 2-D case and $1/\sqrt{t}$ in the 1-D case. In our numerical illustrations, we shall only use the 2-D geometry for both sources and medium.

The smearing of the diffusive solution is the feature preventing any simple reconstruction of the conductivity of the medium. Our chance is that this smearing is controlled by the pseudo-phase function in the asymptotic solution. This chance is also a difficulty: the pseudo-phase might be split into a damping and a phase and the damping be as fast as the oscillation of the phase, preventing any arguments based on the rapid oscillation of the phase term as we shall see for the Hessian estimation in the inversion procedure.

The eikonal equation $[\nabla\tau(\mathbf{x})]^2 = \sigma(\mathbf{x})\mu_0$ allows ray tracing (Červený, Molotkov & Pšenčík 1977) with a 'pseudo-slowness' vector defined by $\mathbf{p} = \nabla\tau$ at each point sampled along the ray. The product $\sigma(\mathbf{x})\mu_0$ can be compacted into one single notation as $u^2(\mathbf{x})$ where u might be called pseudo-slowness. For the eikonal, ray-tracing equations are deduced as soon as a sampling parameter is selected along rays. Let us define s as the curvilinear coordinate on the ray.
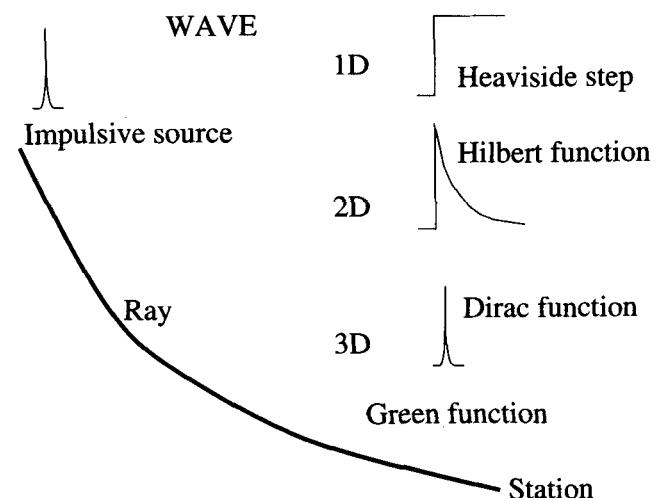

Figure 1. Propagation of the impulsive signal from a source along a ray. Note the difference of shape due to the medium geometry.

DIFFUSION

Impulsive source

Pseudo-ray   3D

1D

2D

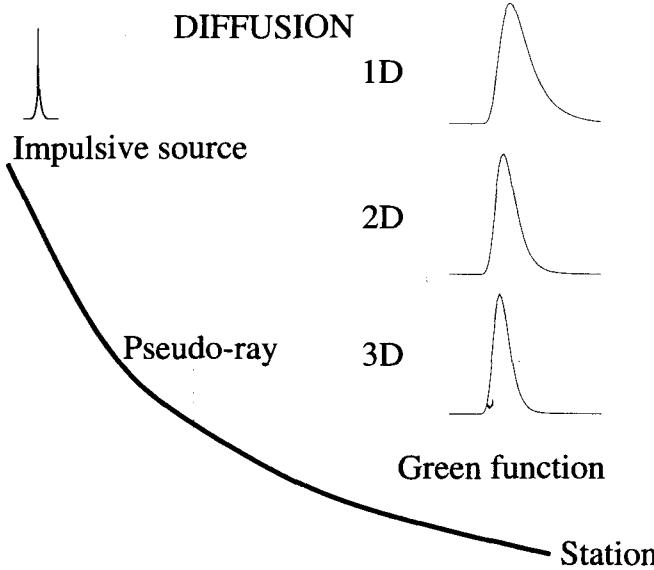**Green function**

Station

Figure 2. Diffusion of the impulsive signal from a source along a pseudo-ray. Note the less dramatic difference of shape compared with wave propagation arising from the medium geometry.

The transport equation which is the second one we are interested in gives the evolution of the amplitude term as we move along the ray. One finds an estimation of the amplitude at s' from s

$$A_0(s') = A_0(s)\frac{\sqrt{u[\mathbf{x}(s)]J(s)}}{\sqrt{u[\mathbf{x}(s')]J(s')}},\tag{12}$$

where J is the Jacobian used in the definition of an elementary surface perpendicular to the ray parameterized by two coordinates γ_1 and γ_2 associated with the curvilinear coordinate s.

The electrical field will be in the frequency domain

$$\frac{1}{\sqrt{u(z)J(z)}}\,e^{-\sqrt{-i\omega}\,\tau(z)}S(\omega)\phi(\gamma_1,\gamma_2),\tag{13}$$

where $S(\omega)$ is the Fourier transform of the time function of the source and ϕ is the intensity of the electromagnetic source. The pseudo-phase τ is equal to $r\sqrt{\mu_0\sigma(r)} = r\,u(r)$.

In order to estimate the intensity ϕ of eq. (13), we might look at a canonical problem where the high-frequency solution is known. Fortunately, a solution given by eq. (8) exists for a homogeneous medium which has been constructed in the previous section. Because the Jacobian is equal to r in a 2-D homogeneous medium, we deduce the intensity for an isotropic source at the origin

$$\phi(\gamma_1,\gamma_2) = \sqrt{2\pi}\tag{14}$$

valid for a smoothly varying medium by identification with the solution (8). The asymptotic solution in a 2-D smooth varying medium for a $\mathbf{r}_s$ source is

$$E_y^0(\mathbf{r},\mathbf{r}_s,\omega) = A_0(\mathbf{r},\mathbf{r}_s)e^{-\sqrt{-i\omega}\,\tau(\mathbf{r},\mathbf{r}_s)}\frac{1}{\sqrt{\sqrt{-i\omega}}}\sqrt{2\pi}\tag{15}$$

where we have again introduced the specific frequency-dependent factor for the 2-D geometry already mentioned in the previous paragraph.

Let us underline again that this solution is only approximate in a 2-D homogeneous medium while the corresponding solution for 1-D and 3-D homogeneous media are exact solutions. Considering asymptotic solutions is a valid assumption, especially when the background medium is nearly homogeneous.

BORN APPROXIMATION

Let us now consider a perturbation of the conductivity. Because in this paper we assume an invariance along the direction y, we consider a 2-D reference medium with a smoothly varying conductivity $\sigma_0(\mathbf{x})$. For a point source (a line source in a 3-D medium with one invariant direction) at the source position $\mathbf{r}_s$, the Green function at position $\mathbf{r}$ is denoted $E_y^0(\mathbf{r},\mathbf{r}_s)$. We want to study media slightly different from this smooth reference medium by a conductivity perturbation given by $\sigma(\mathbf{x}) = \sigma_0(\mathbf{x}) + \Delta\sigma(\mathbf{x})$. We assume that the magnetic permeability μ_0 remains constant. The Green function E_y will be split into the known Green function E_y^0 and the perturbation ΔE_y. The equation

$$\sigma(\mathbf{x})i\omega\mu_0 E_y(\mathbf{r},\mathbf{r}_s) + \nabla^2 E_y(\mathbf{r},\mathbf{r}_s) = -4\pi\delta(\mathbf{r}-\mathbf{r}_s)\tag{16}$$

is expanded into

$$\sigma_0(\mathbf{x})i\omega\mu_0\,\Delta E_y + \nabla^2\,\Delta E_y = -4\pi[i\omega\mu_0\Delta\sigma(\mathbf{x})E_y/4\pi],\tag{17}$$

the solution of which can be written as a convolution of the Green function E_y^0, solution of the left-hand side of eq. (17), and the source term $i\omega\mu_0\,\Delta\sigma(\mathbf{x})E_y/4\pi$ leading to

$$\Delta E_y(\mathbf{r},\mathbf{r}_s,\omega)$$
$$=\frac{i\omega\mu_0}{4\pi}\int_{\mathcal{M}} E_y(\mathbf{r},\mathbf{x},\omega)\,\Delta\sigma(\mathbf{x})E_y^0(\mathbf{x},\mathbf{r}_s,\omega)\,d\mathbf{x}^2,\tag{18}$$

where the domain of integration $\mathcal{M}$ is over diffracting points $\mathbf{x}$. The first-order Born approximation is obtained by replacing E_y with E_y^0 in the integral, leading to a linear functional between $\Delta\sigma$ and ΔE_y:

$$\Delta E_y(\mathbf{r},\mathbf{r}_s,\omega)$$
$$=\frac{i\omega\mu_0}{4\pi}\int_{\mathcal{M}} E_y^0(\mathbf{r},\mathbf{x},\omega)\,\Delta\sigma(\mathbf{x})E_y^0(\mathbf{x},\mathbf{r}_s,\omega)\,d\mathbf{x}^2.\tag{19}$$

Assuming now that solutions have the asymptotic form in the smooth reference 2-D medium

$$E_y^0(\mathbf{x},\mathbf{r}_s,\omega) = A_0(\mathbf{x},\mathbf{r}_s)e^{-\sqrt{-i\omega}\,\tau(\mathbf{x},\mathbf{r}_s)}\frac{1}{\sqrt{\sqrt{-i\omega}}}\sqrt{2\pi}$$

$$E_y^0(\mathbf{r},\mathbf{x},\omega) = E_y^0(\mathbf{x},\mathbf{r},\omega)\tag{20}$$

$$= A_0(\mathbf{r},\mathbf{x})e^{-\sqrt{-i\omega}\,\tau(\mathbf{r},\mathbf{x})}\frac{1}{\sqrt{\sqrt{-i\omega}}}\sqrt{2\pi},$$

we obtain for a given couple of (source, receiver) the simple relation

$$\Delta E_y(\mathbf{r},\mathbf{r}_s,\omega)$$
$$=\frac{i\omega\mu_0}{2}\int_{\mathcal{M}}\Delta\sigma(\mathbf{x})\,A_0(\mathbf{r},\mathbf{x},\mathbf{r}_s)\frac{e^{-\sqrt{-i\omega}\,\tau(\mathbf{r},\mathbf{x},\mathbf{r}_s)}}{\sqrt{-i\omega}}d\mathbf{x}^2,\tag{21}$$

where

$$A_0(\mathbf{r}, \mathbf{x}, \mathbf{r}_s) = A_0(\mathbf{x}, \mathbf{r}_s) A_0(\mathbf{r}, \mathbf{x})$$

$$\tau(\mathbf{r}, \mathbf{x}, \mathbf{r}_s) = \tau(\mathbf{x}, \mathbf{r}_s) + \tau(\mathbf{r}, \mathbf{x}), \tag{22}$$

come from the product of the Green function connecting the source and the diffracting point and the Green function connecting the diffracting point and the receiver.

The asymptotic form has simplified the propagation of the field because ray tracing is symmetrical: the asymptotic Green function from the diffracting point up to the receiver is equivalent to the one from the receiver down to the diffracting point.

Going back to the time domain is possible with a very simple integral expression which is the Fourier inverse of eq. (21):

$$\Delta E_y(\mathbf{r}, \mathbf{r}_s, t) = -\frac{\mu_0}{8\sqrt{\pi}} \int_{\mathcal{M}} \Delta\sigma(\mathbf{x}) A_0(\mathbf{r}, \mathbf{x}, \mathbf{r}_s) \frac{1}{t^{3/2}}$$

$$\times \left[\frac{\tau(\mathbf{r}, \mathbf{x}, \mathbf{r}_s)^2}{t} - 2 \right] e^{-\tau(\mathbf{r},\mathbf{x},\mathbf{r}_s)^2/4t} H(t) \, d\mathbf{x}^2. \tag{23}$$

The kernel of the expression (23) in time has a maximum amplitude at $t_{max} = \tau^2(\mathbf{r})(1/2 + 1/\sqrt{6})$ with a sharper decrease for time lower than t_{max} (exponential term of time) than for time higher than t_{max} (inverse power of time). As a consequence, main contributions to the integral are located on a shell which can be made finite by numerical cut-off of the kernel. We must underline that the situation is slightly more complex than for 2-D seismic imaging: the contribution to the seismogram comes from an isochrone surface along which the image is concentrated and defined by a t equal to traveltime (Bernard & Madariaga 1984; Spudich & Frazer 1984). In diffusive electromagnetic imaging, we have generalized the so-called isochrone property to a less local but still finite shell.

Expressions (21) and (23) are valid in a 2-D or a 3-D medium with an invariance in the y-direction for the definition of the TE mode. Expressions (21) in the frequency domain and (23) in the time domain are our basic linearized forward modelling for which we shall construct an inverse operator. The technique has been previously proposed by Jin *et al.* (1992) based on the work performed by Beylkin (1985) and Beylkin & Burridge (1990) among others on asymptotic Radon transforms.

We check the Born approximation with two simple examples. In the first one, we shall consider a line diffractor of conductivity $\sigma_1 = 0.1\,\mathrm{S\,m^{-1}}$ embedded into a homogeneous medium of conductivity $\sigma_0 = 10^{-2}\,\mathrm{S\,m^{-1}}$. We compute the Born approximation for an incident isotropic line source of unitary strength diffracted by a line located 100 m just below it for frequencies between 10^{-1} Hz and 10^5 Hz. Fig. 3 shows the exact solution compared with the Born asymptotic solution. We must say that the difference in the scattered field arises essentially from the difference between the complete 2-D solution and its high-frequency approximation. As the frequency becomes higher, the discrepancy in amplitude and in phase becomes negligible. In 1-D and 3-D geometries, we should have a perfect agreement because the embedding medium is homogeneous.

In the second example, we compare the solution for a cylinder diffractor at a depth of 100 m in a homogeneous medium of conductivity $0.01\,\mathrm{S\,m^{-1}}$ excited by a line source. We still find a good agreement while we are summing the expression (23) inside the cylinder to recover the diffracted field (Fig. 4). When the conductivity contrast becomes more important, the disagreement between the complete solution and the Born approximation increases at higher frequencies (Fig. 4a). As the cylinder becomes wider, the agreement decreases when the radius increases (Fig. 4b). The Born approximation is valid at relatively high frequencies for
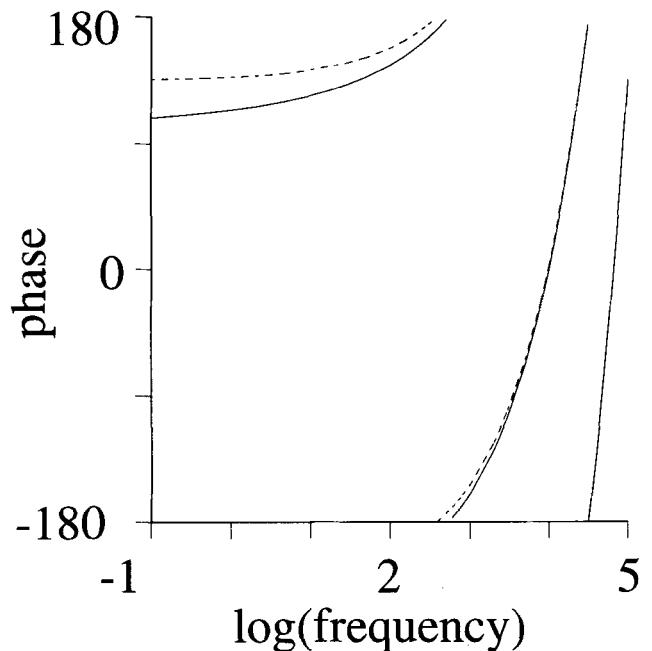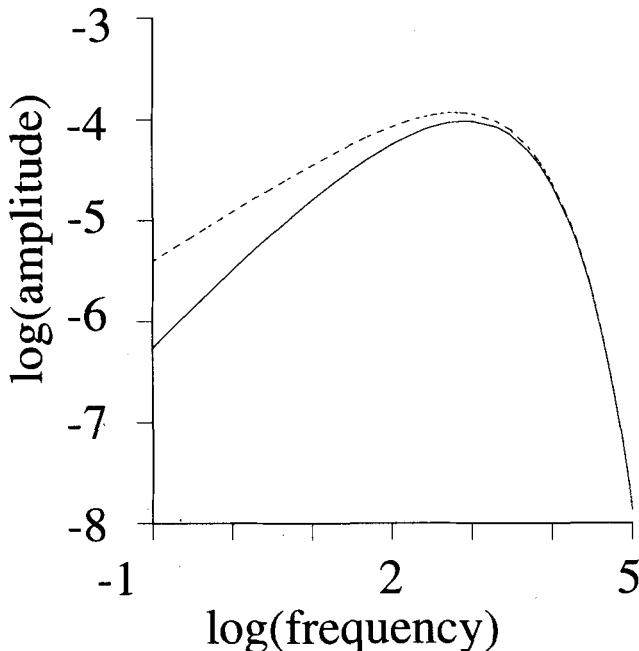

Figure 3. Comparison between the exact solution (solid line) and the asymptotic Born approximation (dashed line) for a line diffractor. The difference arises essentially from the asymptotic approximation. Both amplitude and phases are plotted.
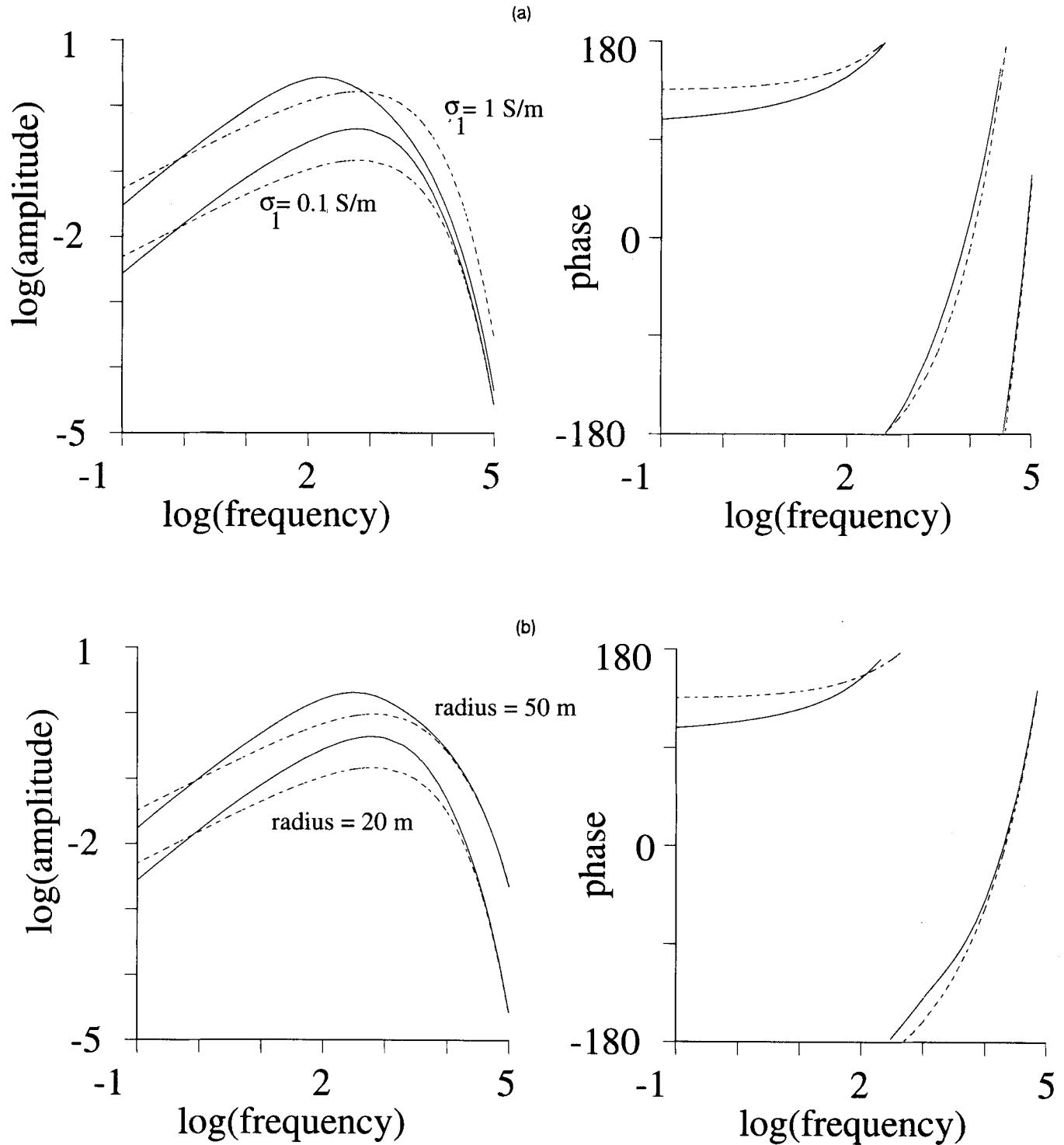
Figure 4. (a) Comparison between the exact solution and the Born approximation for a cylinder diffractor of radius 20 m. Notice the disagreement introduced by the Born approximation when the contrast of conductivity increases. For clarity, only the phase response for the $0.1 \, S \, m^{-1}$ case is included. (b) Comparison between the exact solution and the Born approximation for a cylinder diffractor of conductivity $0.1 \, S \, m^{-1}$. Notice the disagreement introduced by the Born approximation when the size of the cylinder increases. For clarity, only the phase response for the 50 m radius case is included.

small perturbations of the conductivity and for small sizes of diffractor objects. We shall see in our inversion the effects of these disagreements. These effects will be the main limitation of our reconstruction technique.

We must remember that the main misfit arises from our transformation of the 2-D Green function into its high-frequency approximation. For 3-D and 1-D homogeneous media, the Green function agrees with its high-frequency approximation as we have checked. Therefore, we do expect better results with the Born approximation for 3-D structures.

ASYMPTOTIC INVERSION

In order to pose the inverse problem properly we must define both model and data spaces, and the operators between these two spaces. The model space $\mathcal{M}(\mathbf{x})$ is the space of all possible perturbations of the conductivity $\Delta\sigma$ at each point $\mathbf{x}$ of the medium. The data space consists of all electric perturbations of the TE mode for many sources $\mathbf{r}_s$ and receivers $\mathbf{r}$ at different frequencies. For simplicity of the analytical developments, we shall consider Fourier transformed data, but at the end we shall return to the time domain to take advantage of the finite domain of $\mathcal{M}$ from where significant contributions to the electric signal come. This signal is defined on the domain $\mathcal{D}(\mathbf{r}, \mathbf{r}_s, \omega)$. The linearized forward problem can be written in a compact form

$$\Delta E_y = \mathbf{G}\,\Delta\sigma \tag{24}$$

where $\mathbf{G}: \mathcal{M} \to \mathcal{D}$ is the integral operator of the two-way Green functions (see eqs 21 and 23).

The solution of the linearized inverse problem consists of finding the inverse of operator $\mathbf{G}$. We look for an approximate solution to the inversion of eq. (24) by the optimization method which minimizes a misfit function between observed and calculated electric signals (see Tarantola 1987, for a description of inverse theory). We adopt the least-squares norm $\mathcal{L}^2$ of the sum of the square of the difference between observed and predicted signals at each frequency. We shall see that this criterion leads to a quasi-Newtonian iterative method as shown by Jin *et al.* (1992).
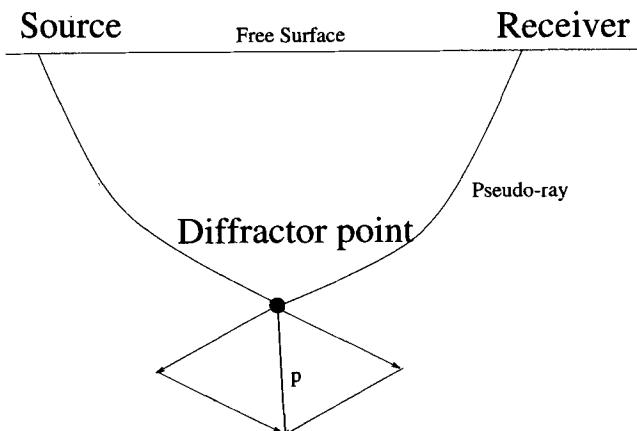

Figure 5. Geometry of pseudo-rays around the diffractor point.

Inversion by a least-squares method

The definition of the misfit function requires an explicit definition of the inner product in data space:

$$\langle \Delta E_y \mid \Delta E_y' \rangle_\mathcal{D} = \sum_{\mathbf{r}_s, \mathbf{r}} \int_\Omega d\omega\, \Delta E_y^*(\mathbf{r}, \mathbf{r}_s, \omega)$$
$$\times \mathbf{Q}(\mathbf{r}, \mathbf{x}_0, \mathbf{r}_s, \omega)\, \Delta E_y'(\mathbf{r}, \mathbf{r}_s, \omega) \tag{25}$$

where $*$ denotes the complex conjugate. The sum and the integral extend over the data space $\mathcal{D}$. The covariance matrix $\mathbf{Q}$ is diagonal by construction with elements:

$$\mathbf{Q}(\mathbf{r}, \mathbf{x}_0, \mathbf{r}_s, \omega) = \frac{|\mathbf{p}(\mathbf{r}, \mathbf{x}_0, \mathbf{r}_s)|^2}{A^2(\mathbf{r}, \mathbf{x}_0, \mathbf{r}_s)} \frac{1}{\sqrt{-i\omega}} \tag{26}$$

where $\mathbf{p}(\mathbf{r}, \mathbf{x}_0, \mathbf{r}_s) = \nabla\tau(\mathbf{r}, \mathbf{x}_0, \mathbf{r}_s)$, is the gradient of the two-way pseudo-phase function τ (Fig. 5).

The particular form of the covariance matrix $\mathbf{Q}$ is introduced in order to correct for the decrease with distance and for the spectral content of the Green function. One can see in the definition of covariance matrix $\mathbf{Q}$ only the influence of the geometrical spreading 'A_0' and not the effect of the diffusion. The covariance matrix depends on $\mathbf{x}_0$, the coordinate of the point at which the model will be inverted. While the choice of a diagonal matrix is rather standard in the optimization method, $\mathbf{Q}$ is usually independent of where we are in the model space. Our choice borrowed from the work done by Jin *et al.* (1992) for seismic profiles is in fact a preconditioning applied to the gradient of the misfit function. The additional complex form of $\mathbf{Q}$ comes from the specific diffusive tail.

The covariance matrix $\mathbf{Q}$ upgrades weak late signals: instabilities might arise when noise exists in the late part of the time signal or when the reference medium leads to strong defocusing in a time window of the signal where energetic pulses are observed. Summing over the data acquisition geometry reduces these incoherent instabilities considerably. If not enough, *a priori* information defining the maximum amplitude for perturbation of conductivity stabilizes the procedure.

For the inverse problem we also need a definition of the inner product between two functions $\Delta\sigma$ and $\Delta\sigma'$ in the model space $\mathcal{M}$:

$$\langle \Delta\sigma \mid \Delta\sigma' \rangle_\mathcal{M} = \int_\mathcal{M} \Delta\sigma^*(\mathbf{x})\, \Delta\sigma'(\mathbf{x})\, d\mathbf{x}^2. \tag{27}$$

The misfit function is defined by

$$S(\Delta\sigma) = 1/2\langle \Delta E_y^{obs} - \mathbf{G}\,\Delta\sigma \mid \Delta E_y^{obs} - \mathbf{G}\,\Delta\sigma \rangle_\mathcal{D}, \tag{28}$$

where ΔE_y^{obs} are the observed data and $\mathbf{G}\,\Delta\sigma$ are the synthetic ones estimated through eq. (24). We formulate the inverse problem as

$$\text{find } \Delta\sigma: \min_{\Delta\sigma} [S(\Delta\sigma)], \tag{29}$$

and we obtain the classical 'system' of normal equations:

$$\mathbf{G}^\dagger\mathbf{G}\,\Delta\sigma = \mathbf{G}^\dagger\,\Delta E_y^{obs} \tag{30}$$

for all $\mathbf{x}$ where $\mathbf{G}^\dagger$ is the adjoint operator to the forward

integral operator G, and defined by the classical relationship

$$\langle \Delta E_v \mid \mathbf{G} \, \Delta\sigma \rangle_{\mathcal{L}} = \langle \mathbf{G}^\dagger \, \Delta E_y \mid \Delta\sigma \rangle_{\mathcal{M}}, \tag{31}$$

while the generalized inverse G^{-g} is equal to $(\mathbf{G}^\dagger \mathbf{G})^{-1} \mathbf{G}^\dagger$.

Estimation of the gradient

The adjoint operator $\mathbf{G}^\dagger$ might be expressed by a kernel $\mathcal{K}$ with the following expression

$$\sum_{\mathbf{r}_s, \mathbf{r}} \int_\Omega d\omega \mathcal{K}(\mathbf{r}, \mathbf{x}, \mathbf{r}_s, \omega) \, \Delta E_y(\mathbf{r}, \mathbf{r}_s, \omega), \tag{32}$$

where the reconstructed function is obtained at position $\mathbf{x}$ assuming a covariance $\mathbf{Q}$ depending on $\mathbf{x}_0$. From eq. (31) and from the forward problem (21),

$$\mathcal{K}(\mathbf{r}, \mathbf{x}, \mathbf{r}_s, \omega)$$

$$= \frac{-1}{2} \mu_0 A(\mathbf{r}, \mathbf{x}, \mathbf{r}_s) \mathbf{Q}^*(\mathbf{r}, \mathbf{x}_0, \mathbf{r}_s, \omega) \sqrt{-i\omega}^* \, e^{-\sqrt{-i\omega}^* \tau(\mathbf{r}, \mathbf{x}, \mathbf{r}_s)}. \tag{33}$$

The formal solution of the system (30) is

$$\Delta\sigma(\mathbf{x}_0) = H^{-1}(\mathbf{x}_0, \mathbf{x}) \gamma^0(\mathbf{x}), \tag{34}$$

where

$$\gamma^0(\mathbf{x}) = \mathbf{G}^\dagger(\mathbf{r}, \mathbf{x}, \mathbf{r}_s) \, \Delta E_y^{\mathrm{obs}}(\mathbf{r}, \mathbf{r}_s, \omega) \tag{35}$$

is the gradient of $S(\Delta\sigma)$ at $\Delta\sigma = 0$ and H is the Hessian giving the information of the curvature of the misfit function. Explicitly the gradient is given by

$$\gamma 0(\mathbf{x}) = \frac{-\mu_0}{2} \sum_{\mathbf{r}_s, \mathbf{r}} \int_\Omega d\omega \frac{A(\mathbf{r}, \mathbf{x}, \mathbf{r}_s)}{A^2(\mathbf{r}, \mathbf{x}_0, \mathbf{r}_s)}$$

$$\times |\mathbf{p}(\mathbf{r}, \mathbf{x}_0, \mathbf{r}_s)|^2 \, e^{-\sqrt{-i\omega}^* \tau(\mathbf{r}, \mathbf{x}, \mathbf{r}_s)} \Delta E_y^{\mathrm{obs}}(\mathbf{r}, \mathbf{r}_s, \omega) \tag{36}$$

in the frequency domain. Expressing $\Delta E_y^{\mathrm{obs}}(\mathbf{r}, \mathbf{r}_s, \omega)$ as the Fourier transform of $\Delta E_y^{\mathrm{obs}}(\mathbf{r}, \mathbf{r}_s, t)$ leads to the following expression:

$$\gamma^0(\mathbf{x}) = -\frac{\mu_0}{2} \sum_{\mathbf{r}_s, \mathbf{r}} \int_T dt \, \Delta E_y^{\mathrm{obs}}(\mathbf{r}, \mathbf{r}_s, t) \frac{A(\mathbf{r}, \mathbf{x}, \mathbf{r}_s)}{A^2(\mathbf{r}, \mathbf{x}_0, \mathbf{r}_s)} \times |\mathbf{p}(\mathbf{r}, \mathbf{x}_0, \mathbf{r}_s)|^2$$

$$\times \int_\Omega d\omega' e^{-\sqrt{-i\omega'} \tau(\mathbf{r}, \mathbf{x}, \mathbf{r}_s)} e^{-i\omega' t}. \tag{37}$$

We have used the complex conjugate operation giving $\sqrt{-i}^* = \sqrt{i}$ and the transformation of ω into $\omega' = -\omega$. By doing so, we are able to write the gradient as a single integral in the time domain

$$\gamma^0(\mathbf{x}) = -\frac{u_0 \sqrt{\pi}}{2} \sum_{\mathbf{r}_s, \mathbf{r}} \frac{A(\mathbf{r}, \mathbf{x}, \mathbf{r}_s)}{A^2(\mathbf{r}, \mathbf{x}_0, \mathbf{r}_s)} |\mathbf{p}(\mathbf{r}, \mathbf{x}_0, \mathbf{r}_s)|^2$$

$$\times \int_T dt \, \Delta E_y^{\mathrm{obs}}(\mathbf{r}, \mathbf{r}_s, t) \frac{\tau(\mathbf{r}, \mathbf{x}, \mathbf{r}_s)}{t^{3/2}} e^{-\tau(\mathbf{r}, \mathbf{x}, \mathbf{r}_s)^2/4t} H(t). \tag{38}$$

The time-domain integration in the asymptotic inversion kernel is around $t_{\mathrm{max}} = \tau(\mathbf{r}, \mathbf{x}, \mathbf{r}_s)^2/2$ which corresponds to a shell in the diffraction domain $\mathcal{M}$. We have found the equivalent of the isochrone summation for the asymptotic seismic migration related to the principle of coinciding time of Claerbout (1985). Apart from an integration over a time interval instead of a single value for seismic migration, we have an expression that is manageable for practical implementation.

Let us underline that the choice of the factor $\mathbf{Q}$ has modified the t_{max} compared with the one obtained for the forward linearized expression.

Asymptotic expression of the Hessian

The operator H^{-1} in eq. (34) is the formal inverse of $G^\dagger G$ and is very difficult to estimate for many inverse problems (see Jin *et al.* 1992, for a short discussion and Tarantola 1987, for an extensive review). In our approach, an asymptotic estimation is possible. We found from eqs (21) and (32) that

$$H(\mathbf{x}, \mathbf{x}_0) = \frac{\mu_0^2}{4} \sum_{\mathbf{r}_s, \mathbf{r}} \frac{A(\mathbf{r}, \mathbf{x}, \mathbf{r}_s)}{A(\mathbf{r}, \mathbf{x}_0, \mathbf{r}_s)} |\mathbf{p}(\mathbf{r}, \mathbf{x}_0, \mathbf{r}_s)|^2$$

$$\times \int_\Omega d\omega \sqrt{-i\omega} \, e^{-\sqrt{-i\omega}^* \tau(\mathbf{r}, \mathbf{x}, \mathbf{r}_s) - \sqrt{-i\omega} \tau(\mathbf{r}, \mathbf{x}_0, \mathbf{r}_s)}, \tag{39}$$

which reduces to

$$H(\mathbf{x}, \mathbf{x}_0) = \frac{\mu_0^2}{4} \sum_{\mathbf{r}_s, \mathbf{r}} \frac{A(\mathbf{r}, \mathbf{x}, \mathbf{r}_s)}{A(\mathbf{r}, \mathbf{x}_0, \mathbf{r}_s)} |\mathbf{p}(\mathbf{r}, \mathbf{x}_0, \mathbf{r}_s)|^2$$

$$\times \int_0^\infty d\omega \sqrt{2\omega} \, e^{-\sqrt{\omega/2}[\tau(\mathbf{r}, \mathbf{x}_0, \mathbf{r}_s) + \tau(\mathbf{r}, \mathbf{x}, \mathbf{r}_s)]}$$

$$\times [\cos\{\sqrt{\omega/2}[\tau(\mathbf{r}, \mathbf{x}, \mathbf{r}_s) - \tau(\mathbf{r}, \mathbf{x}_0, \mathbf{r}_s)]\}$$

$$- \sin\{\sqrt{\omega/2}[\tau(\mathbf{r}, \mathbf{x}, \mathbf{r}_s) - \tau(\mathbf{r}, \mathbf{x}_0, \mathbf{r}_s)]\}]. \tag{40}$$

The term under the integral over frequency has a damping term which prevents any arguments of equally balanced contributions for the whole frequency spectrum as it is for seismic inversion. This is a fundamental difference that we have underlined previously but we can argue that the main contribution to the integral is when the phase of the exponential is zero because the diffusive damping term is a slowly decaying function. If the background medium is sufficiently smooth, this occurs when $\mathbf{x}$ is close to $\mathbf{x}_0$. With local expansion of the pseudo-phase and the amplitude

$$\tau(\mathbf{r}, \mathbf{x}, \mathbf{r}_s) \sim \tau(\mathbf{r}, \mathbf{x}_0, \mathbf{r}_s) + \mathbf{p} \cdot (\mathbf{x} - \mathbf{x}_0)$$

$$A(\mathbf{r}, \mathbf{x}, \mathbf{r}_s) \sim A(\mathbf{r}, \mathbf{x}_0, \mathbf{r}_s) \tag{41}$$

we find the asymptotic expression of the Hessian H

$$H(\mathbf{x}, \mathbf{x}_0) \sim \frac{\mu_0^2}{4} \sum_{\mathbf{r}_s, \mathbf{r}} |\mathbf{p}(\mathbf{r}, \mathbf{x}_0, \mathbf{r}_s)|^2$$

$$\times \int_0^\infty d\omega \sqrt{2\omega} \, e^{-\sqrt{2\omega} \tau(\mathbf{r}, \mathbf{x}_0, \mathbf{r}_s)} e^{-\sqrt{\omega/2} \mathbf{p} \cdot (\mathbf{x} - \mathbf{x}_0)}$$

$$\times \{\cos[\sqrt{\omega/2} \, \mathbf{p} \cdot (\mathbf{x} - \mathbf{x}_0)]$$

$$- \sin\sqrt{\omega/2} \, \mathbf{p} \cdot (\mathbf{x} - \mathbf{x}_0)]\} \tag{42}$$

which has significant values when $\mathbf{x}$ is close to $\mathbf{x}_0$. We shall assume the more drastic approximation,

$$H(\mathbf{x}, \mathbf{x}_0) \sim H(\mathbf{x}_0, \mathbf{x}_0) \delta(\mathbf{x} - \mathbf{x}_0), \tag{43}$$

justified by the exponential decrease away from the position $\mathbf{x}_0$. The Hessian can now be estimated as

$$H(\mathbf{x}, \mathbf{x}_0) \sim \delta(\mathbf{x} - \mathbf{x}_0) \frac{\mu_0^2}{2} \sum_{\mathbf{r}_s, \mathbf{r}} |\mathbf{p}(\mathbf{r}, \mathbf{x}_0, \mathbf{r}_s)|^2 \frac{1}{\tau^3(\mathbf{r}, \mathbf{x}_0, \mathbf{r}_0)}. \tag{44}$$

The final and precise shape of the operator H is mainly controlled by the data acquisition geometry and eq. (44) should be considered only as an estimation for an iterative inversion method. The nearly diagonal structure of the operator H makes the computation of the inverse easier and leads to

$$\Delta\sigma(\mathbf{x}_0) = 1/H(\mathbf{x}_0, \mathbf{x}_0)\; \gamma_0(\mathbf{x}_0).\tag{45}$$

In order to check the final gradient expression (38) and the final Hessian expression (44), we have computed the reconstructed conductivity at a single diffracting point $\mathbf{x}_0$ from the scattered field computed by the Born approximation. We have deduced the exact conductivity contrast between the homogeneous reference medium and the scattering point. This analytical checking makes us confident in our expressions for imaging diffusive fields.

Iterative quasi-Newton inversion method

Let us note h the approximation of the Hessian H. The quasi-Newton solution of the inverse problem (29) is

$$\Delta\sigma(\mathbf{x})^{n+1} = \Delta\sigma(\mathbf{x})^n + h^{-1}\gamma^n \tag{46}$$

where γ^n is the gradient of the misfit function $S(\Delta\sigma)$ calculated around the value of $\Delta\sigma$ at the nth iteration:

$$\gamma^n = G^\dagger(\Delta E^{\text{obs}} - G\,\Delta\sigma^n).\tag{47}$$

As shown by Jin *et al.* (1992), the iterative method converges to the limit

$$\lim_{n\to\infty} \Delta\sigma^n = (\mathbf{G}^{-g}\mathbf{G})^{-1}\mathbf{G}^{-g}\,\Delta E^{\text{obs}}\tag{48}$$

which shows that the iterative method corrects for any bias in the Hessian estimation.

A self-consistent test

Before performing an inversion for a complete solution, we want to test the internal coherence of the linear inversion we propose. We have computed the Born approximation for a cylinder of radius 20 m at a depth of 100 m. The conductivity

of the cylinder is $0.1\,\mathrm{S\,m^{-1}}$ embedded in a homogeneous medium of conductivity $0.01\,\mathrm{S\,m^{-1}}$. We consider a single line source right above the cylinder and five receivers at the free surface distributed by steps of 50 m on both sides of the source.

Figure 6 shows both the true cylinder and the recovered conductivity contrast. The recovered maximum value is only $0.01\,\mathrm{S\,m^{-1}}$ while we should have found a value around $0.09\,\mathrm{S\,m^{-1}}$. The wider extension of the recovered image explains this low maximum value. With the blurred image of Fig. 6, the predicted signals can explain most parts of the synthetic signals. Unfortunately, this is a drawback of the diffusion phenomenon which implies an integration over a pseudo-isochrone shell to recover the image. We find the typical 'smile' associated with the data acquisition geometry. During iterations, the misfit function decreases from 130 at the first iteration down to 66 at the 50th iteration.

If we consider other sources translated on the horizontal axis, we are able to stack different pictures of the medium and to improve our resolution. The cylinder shape is better resolved as expected in Fig. 7 with a noticeable reduction of the 'smile'. The misfit function goes down to 44 when normalized by the number of sources, lower than the misfit function for a single source. The extension of the recovered image still biases strongly the maximum amplitude of the conductivity contrast. We do expect better results when considering other geometries than the surface-to-surface geometry.

A test with the analytical complete solution

The previous test has been performed using Born computation as synthetic data. What happens when considering the exact solution of diffusion by a cylinder? We have already compared true and Born solutions in the frequency domain in a previous paragraph. From these analytical solutions in the frequency domain, we compute the solution in the time domain for the same geometry by fast Fourier transform. Then, we perform asymptotic inversions similar to the ones previously computed with Born synthetic solutions.
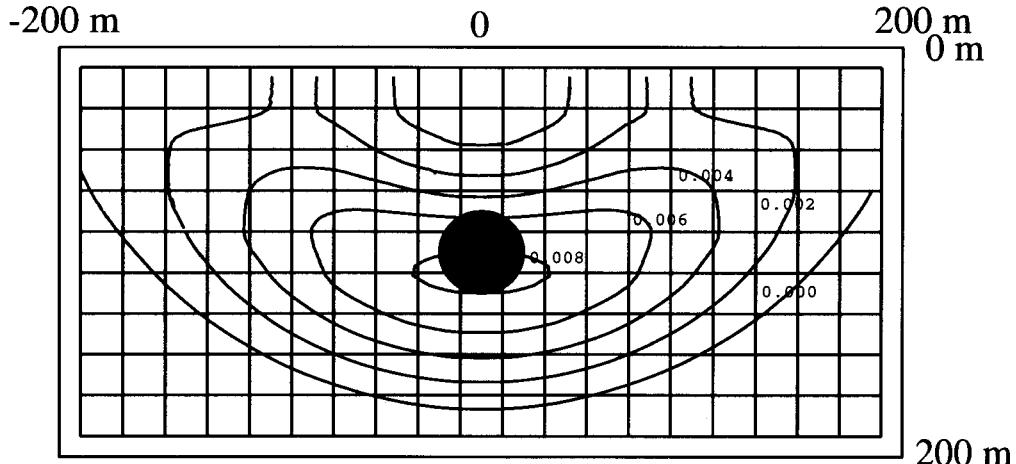

Figure 6. Conductivity contrast recovered after 50 iterations for one source at the free surface above the cylinder. Inverted data are the Born solution.
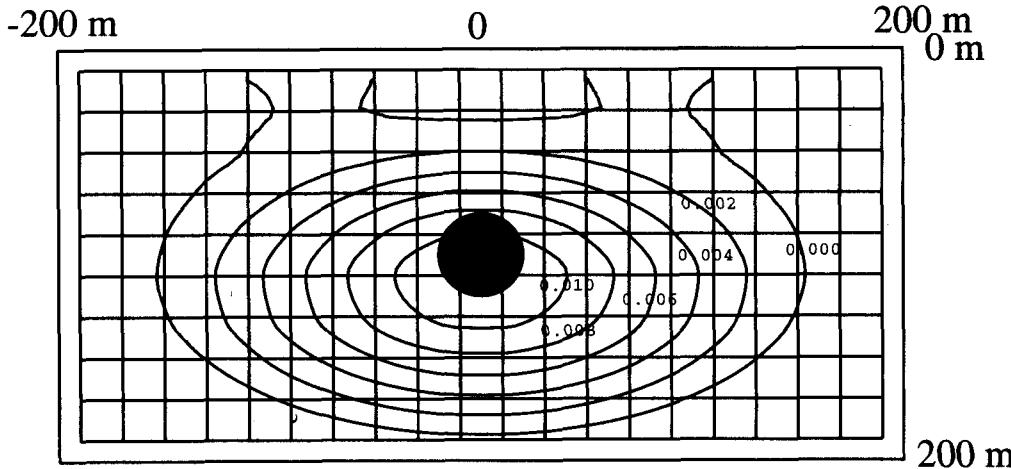
Figure 7. Conductivity contrast recovered after 50 iterations for five sources distributed at the free surface on both sides of the cylinder. Inverted data are the Born solution.

For inversion of the exact solution by a scattering cylinder, we find a deeper image with the typical 'smile' associated with one source geometry (see Fig. 8). The maximum amplitude of conductivity contrast is as high as 0.03 S m^{-1}. The amplitude difference between the Born solution and the complete solution in the time domain easily explains this amplification (see Fig. 9). The slight shift of the maximum diffusion pulse between these two solutions explains also why the image is deeper than the true cylinder. The reduction of the misfit function is from 475 at the first iteration to 166 at the 50th iteration. Fig. 9 gives an example of the residual signal left unexplained by the analytical inversion.

Performing the inversion using more sources removes the 'smile' geometry as shown in Fig. 10 but does not improve the position of the strongest conductivity amplitude which is still deeper than the true position. Changing the geometry structure by adding data recorded inside wells might improve this position problem already noticed with the Born approximation and amplified when using the exact solution.

We see in this final synthetic example the difficulty inherent in diffusion phenomena which blurs the image by the spatial extension of the so-called pseudo-isochrone shell for image recovering. This distortion of the image arises also from the Born approximation which, at intermediate frequencies, shows relatively poor agreement. Starting from a better reference medium with the already included low-frequency content of the conductivity might improve the picture, because, for the relatively higher spatial frequencies, the associated diffusion tail in time will be easier to handle.

DISCUSSION AND CONCLUSION

We have developed an analytical inversion for diffusive electromagnetism. This formalism draws its features from the seismic inversion approach. We extend the isochrone line concept of wave propagation to a pseudo-isochrone shell concept for diffusion. By doing so, we were able to construct an inversion scheme with explicit formula for the gradient and the Hessian of the misfit function. Because these formula are analytical, they are insensitive to noise
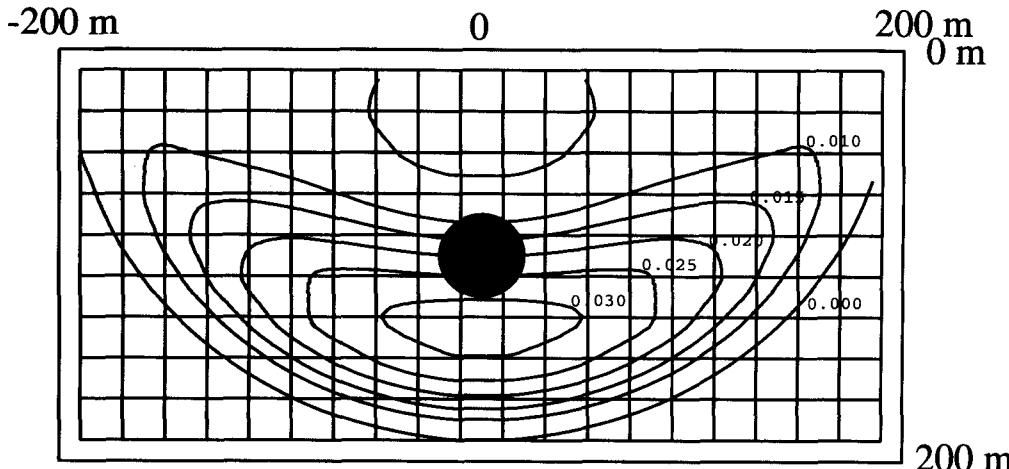

Figure 8. Conductivity contrast recovered after 50 iterations for one source at the free surface above the cylinder. Inverted solution is the exact analytical solution.
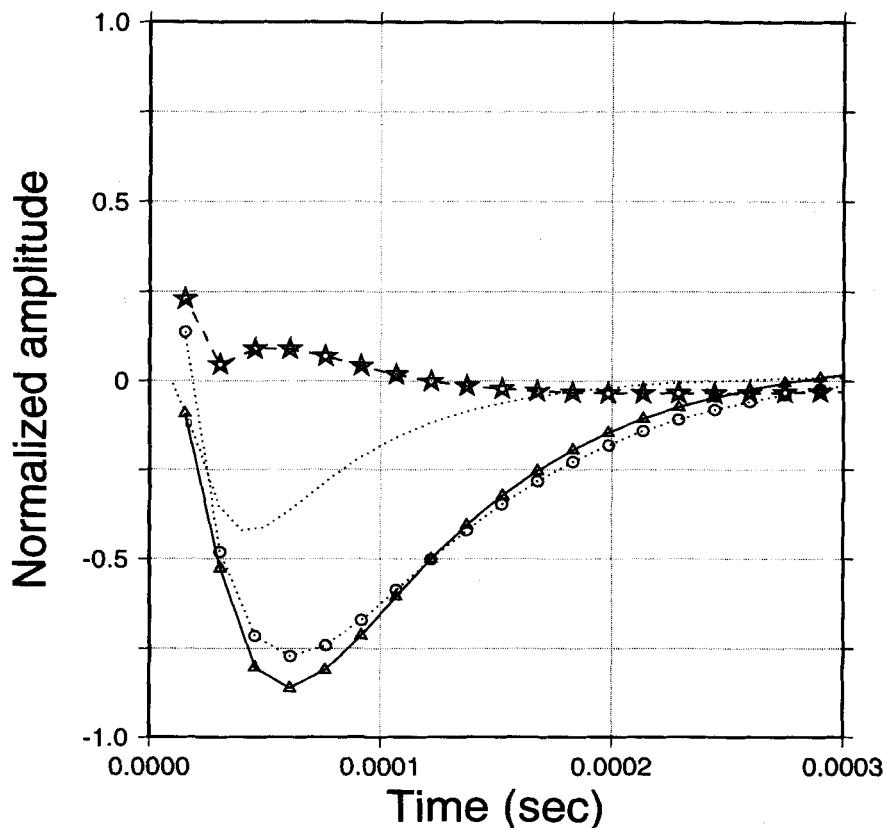
Figure 9. Synthetic electric signal (triangles) recorded at the receiver above the cylinder as well as the predicted signal (circles) computed for the cylinder image. The residual is also shown (diamonds), as well as the synthetic Born solution used in the forward modelling (dots).

which are simply not focused back into the medium when incoherent as already shown for seismic data (Lambaré *et al.* 1992).

The use of the Born approximation has limitations when we try to recover a spatially extended object on a homogeneous background. The possible extension to a smooth inhomogeneous reference medium will improve the position of heterogeneities by requiring only a fit of the relatively high-frequency part of the electric signal when the smooth background velocity has already been obtained. In

that sense, this reconstruction technique is only a partial one in terms of spatial resolution.

In any case, we believe that, because the main diffusion pulse which is the one fitted in our present applications would have been already contained in our initial model, the spatially high-frequency content of the image will be better resolved. Of course, we might analyse the effect of noise for this inversion scheme as well as we might analyse performances on real data. This will be the purpose of object work.
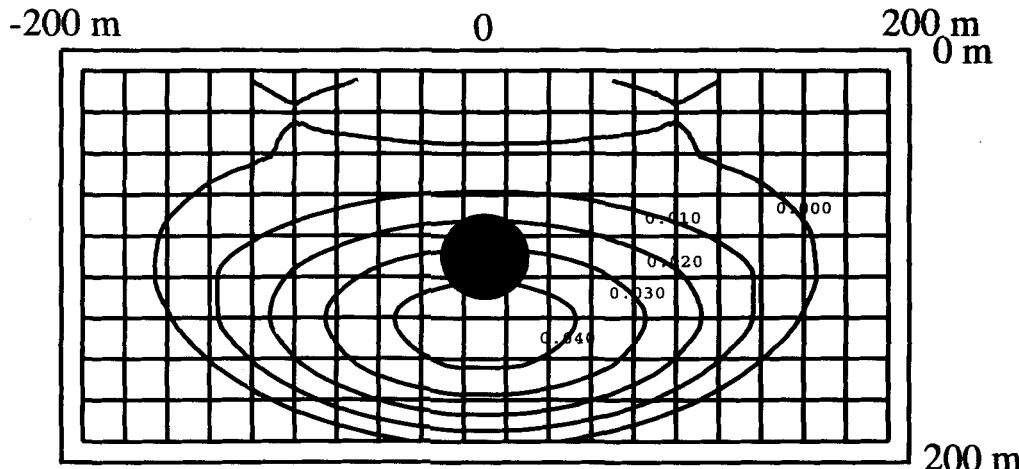

Figure 10. Conductivity contrast recovered after 50 iterations for five sources distributed at the free surface on both sides of the cylinder. The inverted solution is the exact analytical solution.

ACKNOWLEDGMENTS

REFERENCES

Aki, K. & Richards, P., 1980. *Quantitative Seismology: Theory and Methods*, W. H. Freeman and Co, San Francisco, CA.

Barnett, C.T., 1984. Simple inversion of time-domain electromagnetic data, *Geophysics*, **49**, 925–933.

Bernard, P. & Madariaga, R., 1984. A new asymptotic method for the modelling of near-field accelerograms, *Bull. seism. Soc. Am.*, **74**, 539–559.

Beylkin, G., 1985. Imaging of discontinuities in the inverse scattering problem by inversion of a causal generalized Radon transfrom, *J. math. Phys.*, **26**, 99–108.

Beylkin, G. & Burridge, R., 1990. Linearized inverse scattering problems in acoustics and elasticity, *Wave Motion*, **12**, 15–52.

Bleistein, N., 1984. *Mathematical Methods for Wave Phenomena*, Academic Press, Inc., Orlando, FL.

Borovikov, V.A. & Kinber, B.Y.E., 1974. Some problems in the asymptotic theory of diffraction, *Proc. IEEE*, **62**, 1416–1437.

Cagniard, L., 1953. Basic theory of the magneto-telluric method of geophysical prospecting, *Geophysics*, **18**, 605–635.

Carslaw, H.S. & Jaeger, J.C., 1978. *Conduction of Heat in Solids*, Oxford University Press, Oxford.

Červený, V., Molotkov, I.A. & Pšenčík, I., 1977. *Ray Method in Seismology*, Charles University Press, Prague.

Chapman, C.H., 1985. Ray theory and its extension: WKBJ and Maslov seismograms, *J. Geophys.*, **58**, 27–43.

Choudhary, S. & Felsen, L.B., 1973. Asymptotic theory for inhomogeneous waves, *IEEE Trans. Antennas Propag.*, **AP-21**, 827–842.

Claerbout, J.F., 1985. *Imaging the Earth's Interior*, Blackwell, Oxford.

Davis, D.T., Lytle, R.J. & Laine, E.F., 1979. Use of high-frequency electromagnetic waves for mapping an in situ coal gasification burn front, *In situ*, **3**, 95–119.

Gibert, D. & Virieux, J., 1991. Electromagnetic imaging and simulated annealing, *J. geophys. Res.*, **96**, 8057–8067.

Jin, S., Madariaga, R., Virieux, J. & Lambaré, G., 1992. Two-dimensional asymptotic iterative elastic inversion, *Geophys. J. Int.*, **108**, 575–588.

Lambaré, G., Virieux, J., Madariaga, R. & Jin, S., 1992. Iterative asymptotic inversion: applications for one parameter, *Geophysics*, **57**, 1138–1154.

Lee, K.H. & Xie, G., 1993. A new approach to imaging with low-frequency electromagnetic fields, *Geophysics*, **58**, 780–796.

Lee, S., McMechan, G.A. & Aiken, C.L., 1987. Phase-field imaging: the electromagnetic equivalent of seismic migration, *Geophysics*, **52**, 1678–693.

Lee, K.H., Liu, G. & Morrison, H.F., 1989. A new approach to modeling the electromagnetic response of conductive media, *Geophysics*, **54**, 1180–1192.

Levy, S., Oldenburg, D.W. & Wang, J., 1988. Subsurface imaging using magnetotelluric data, *Geophysics*, **53**, 104–117.

Ludwig, D., 1966. Uniform asymptotic expansion at a caustic, *Commun. Pure appl. Math.*, **29**, 215–250.

Nekut, A.G., 1994. Electromagnetic ray-trace tomography, *Geophysics*, **59**, 371–377.

Radcliff, R.D. & Balanis, C.A., 1981. Electromagnetic geophysical imaging incorporating refraction and reflection, *IEEE Trans. Antennas Propag.*, **AP-29**, 288–292.

Smith, J.T., 1988. Rapid inversion of multi-dimensional magnetotelluric data, *PhD thesis*, University of Washington.

Spudich, P. & Frazer, L.N., 1984. Use of ray theory to calculate high-frequency radiation from earthquake sources having spatially variable rupture velocity and stress drop, *Bull. seism. Soc. Am.*, **74**, 2061–2082.

Tarantola, A., 1987. *Inverse Problem Theory*, Elsevier Science Publishers BV, Amsterdam.

Tarits, P., 1989. Contribution des sondages électromagnétiques profonds à l'étude du manteau supérieur terrestre, *Thèse d'État*, Université Paris 7.

Tikhonov, A.N., 1965. Mathematical basis of the theory of electromagnetic soundings, *Zh. Vychisl. Mat. Mat. Fiz.*, **5**, 545–548.

Tripp, A.C., Hohmann, G.W. & Swift, C.M., 1984. Two-dimensional resistivity inversion, *Geophysics*, **49**, 1708–1717.

Wait, J.R., 1981. *Wave Propagation Theory*, Pergamon Press, Oxford.

Weidelt, P., 1972. The inverse problem of geomagnetic induction, *J. Geophys.*, **38**, 257–289.

Weidelt, P., 1975, Inversion of two-dimensional conductivity structures, *Phys. Earth planet. Inter.*, **10**, 282–291.

Zhdanov, M.S., 1988. *Integral Transforms in Geophysics*, p. 367, Springer Verlag, Berlin.

Zhdanov, M.S. & Frenkel, M.A., 1983. The solution of the inverse problems on the basis of the analytical continuation of the transient electromagnetic field in the reverse time., *J. Geomagn. Geoelect.*, **35**, 747–765.

Zhdanov, M.S. & Booker, J.R., 1993. Underground imaging by electromagnetic migration, *SEG Expanded Abstracts*, pp. 81–82, 63rd Annual Meeting, Soc. Explor. Geophys., Washington, DC.

Zhdanov, M.S. & Keller, G., 1994. *The Geoelectrical Methods in Geophysical Exploration*, p. 873, Elsevier, Amsterdam, London, New York, Tokyo.